

PREDICTION OF TURBOMACHINERY FLOW PHYSICS FROM CFD – REVIEW OF RECENT COMPUTATIONS OF APPACET TEST CASES

DAVID G. GREGORY-SMITH AND SUE C. CROSSLAND

*School of Engineering, University of Durham,
South Road, DH13LE Durham, UK
d.g.gregory-smith@durham.ac.uk*

(Received 5 July 2001)

Abstract: In order to maintain a competitive edge, the turbomachinery industry has to rely increasingly on design and analysis methods based on numerical simulation of flow. The European funded APPACET was set up to study the application of turbulence modelling and the simulation of unsteady interactions to provide guidelines for the application of CFD to design. This paper shows the results of computations of four of the test cases studied by the project. The importance of grid refinement has been clearly demonstrated, but no evidence was found that one family of turbulence models could be definitely better than the other. Compared to steady results, unsteady time-averaged solutions have not shown any major improvement in accuracy. However unsteady flow phenomena generating losses within each blade row have been captured and partly explained.

Keywords: turbomachinery, CFD, turbulence modelling, grid dependence, unsteady interaction

1. Introduction

Industrial designers of turbomachinery, either for aerospace or power generation applications, require challenging technological advances in order to improve or retain their competitive position. Machine performance will have to increase substantially in the years to come: lower bulk and weight, higher efficiency, reduced wear-related loss of performance and improved handling characteristics, including operation at off-design conditions. This level of performance will also have to be achieved within shorter development time scales and tighter budgets. In order to tackle these issues, industry relies increasingly on numerical modelling for guidance and design.

Turbomachinery design has benefited largely in recent years from 3D Navier-Stokes solvers. Compressors are particularly sensitive to blade and endwall blockage, shock boundary layer interactions or hub-corner stall separation. These effects can only be predicted through full 3D turbulent modelling but their detailed prediction can be quite sensitive to turbulence models. Also, it is largely recognised that unsteady blade row interactions affect global performance at design and off-design conditions. Among the most significant effects are the interaction of the wakes with the downstream blade row, the

unsteady inter-action of the rotor overtip leakage flow with the shroud endwall flow in the downstream stator and the influence of the rotor endwall flow on the subsequent stator corner stall. Although, various unsteady loss mechanisms have been suggested, there is no established understanding of these effects, nor is it known how to model them within quasi-steady, design oriented, simulation tools of multiple blade row interactions.

To address the problems of applying turbulence modelling and unsteady interactions, the European funded APPACET (Assessment of Physical Processes And Code Evaluation for Turbomachinery flows) programme was set up. Its aim was the understanding, evaluation and modelling of the main unsteady loss sources in rotor/stator interactions. This was to be achieved through new advanced experimental data coupled to systematic and controlled numerical simulations, with the object to provide the designer with modelling guidelines. Unsteady phenomena are dependent on turbulent and eventually transition effects, but it was not considered feasible at the present to assess the validity of turbulence models on unsteady data. So the effort was directed to steady simulations of test cases representative of the complex 3D flow structure of advanced machines, with the expectations that the most appropriate “steady” turbulence models will be valid for the unsteady flow simulations.

This paper aims at reviewing the results of the computational aspects of the programme, specifically how they compared to the experimental data for four of the five test cases.

2. The APPACET Project

The APPACET Project contained 10 partners:

Vrije Universiteit Brussels (VUB), Belgium (Coordinator)
ABB-ALSTOM, U. K. (now Alstom Energy)
Ecole Centrale de Lyon, France (ECL)
DLR, Germany
LEMF I at Université de Paris VI, France (UPMC)
FIAT Avio S. P. A., Italy
SNECMA Moteurs, France
National Technical University of Athens, (NTUA)
University of Firenze, Italy (UF)
University of Durham, UK (UD)

The project started in January 1998 and finished in July 2000. The work was centred around 5 Test Cases, some of which required data to be taken as part of the project. All the test cases were computed by several partners. An outline of each test case is made below:

Test Case 1: NTUA Annular Compressor Cascade

This consists of a compressor cascade with a hub tip clearance that is variable. The hub can be rotated to give relative motion between the blade tip and the hub. NTUA obtained new data with pneumatic probes and laser Doppler anemometry upstream, within and downstream of the blade row. The partners involved in computations were VUB, UPMC, SNECMA and NTUA

Test Case 2: NASA Transonic Rotor37

This is a transonic fan rotor and is well known as a test case for the evaluation of CFD. The following partners performed computations of the flow, VUB, ABB, ECL, DLR, UPMC, NTUA and UF.

Test Case 3: ECL4 Axial Supersonic Compressor Stage

A new supersonic compressor stage from SNECMA was tested at ECL. Partners involved in computations were ECL, SNECM, VUB, UF and UPMC. However because of commercial confidentiality, the test case is not discussed in this paper.

Test case 4: DLR Contra-Rotating Fan

The transonic contra-rotating research fan CRISP (Counter Rotating Integrated Shrouded Propfan) was designed by the German manufacturer MTU and tested by DLR. The fan consists of two rotors which rotate in opposite directions with 10 and 12 blades for the first and second rotors. The test case provides data on blade row interactions with both wakes and shock waves. It considers a 2D plane at 60% span with stream-tube thickness variation specified from a quasi-steady 3D computation. Computations were performed by ABB, DLR and UF.

Test case 5: The Axial 1-1/2 Turbine Stage From Aachen

This well known test case consists of a stator, rotor and stator operating in an axial configuration with modest Mach numbers (~ 0.5). The aspect ratio of the blades is low and there are significant secondary flows and a tip clearance vortex. Partners who calculated this highly three dimensional flow were ABB, FIAT, UPMC and VUB.

The objectives of the project were implemented through four separate steps:

- Validation of turbulence models on steady single blade row test cases (Test Cases 1 and 2). This objective focused on tip clearance-secondary flow interactions in steady conditions by controlled monitoring of the separate effects of grid dependence and turbulence models.
- Gaining a better understanding of the unsteady multiple blade row interactions in axial compressor stages by the collection of new data using advanced instrumentation on heavily instrumented rigs of industrial relevance, with two sets of new experiments (Test Cases 3 and 4). The experimental work was coupled to full unsteady simulations on fine grids of high resolution.
- Based on the most adequate turbulence models from the validation task on the steady test cases, improving modelling capabilities of quasi-steady and full unsteady rotor/stator interaction models, focusing on issues of identification and quantification of dominant unsteady loss sources (Test Cases 3, 4 and 5).
- Action towards dissemination and communication, involving a data base initiative and a workshop, through a strong connection to existing European scientific and industrial networks. Although outside the time scale of the project, this paper is a continuing legacy of this objective.

3. The annular compressor cascade

The high speed annular cascade test facility developed at NTUA was designed specifically to simulate the flow at the tip of a rotor at the rear of an axial high pressure compressor, where tip clearance effects have the strongest influence on the flow structure. A brief description of the test facility is given here, and a schematic is shown in Figure 1. A more detailed description is given in Mathiodakis *et al.* [1]. To avoid the associated problems of measurements in rotating blade passages, a stationary blade with a rotor aerofoil is used, with an inner wall rotating from pressure to suction sides to simulate the relative flow between the blade tip and the flowpath wall. A spiral casing (scroll) creates the inlet

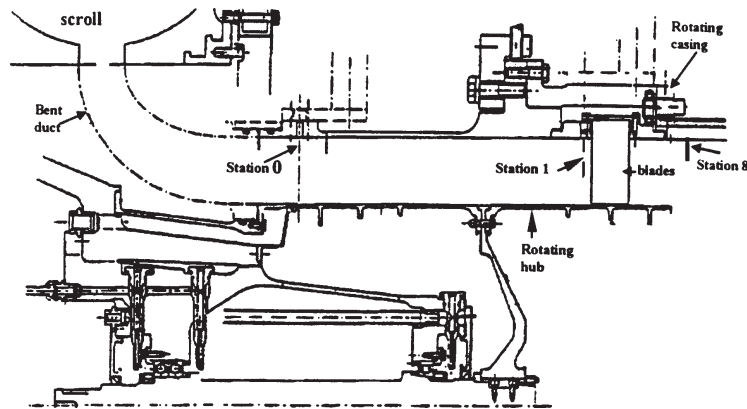


Figure 1. Schematic of the NTUA annular cascade test facility

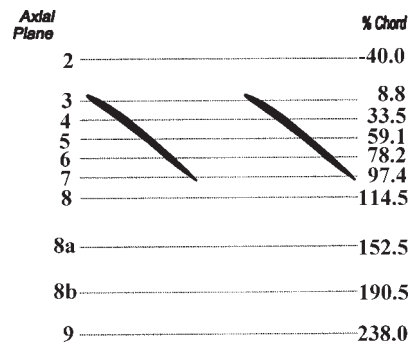


Figure 2. Nomenclature for the measurement planes for the NTUA annular cascade

swirl to the cascade. The flowpath is cylindrical, and the blades are straight and cantilevered (fixed on the casing with a clearance gap at the rotating inner wall). The final part of the inner wall (at 198% axial chord from the leading edge) does not rotate.

To provide comprehensive flowfield information, two types of measurements were performed:

- Inlet and outlet flow distribution measurements were performed using 5-hole probes, providing information on the 3D flow field and characterizing the cascade performance.
- Detailed measurements were made inside the blade passage using 5 hole probes at 3 axial locations (33%, 78% and 115% axial chord from the leading edge, *i.e.* planes 4, 6 and 8, as illustrated in Figure 2) providing velocity vector and total and static pressure information, and 3D Laser Doppler Velocimetry (LDV) measurements at 5 axial locations (8%, 33%, 59% 78% and 97% axial chord from the leading edge, *i.e.* at planes 3–7) provide information on the three velocity components and turbulence quantities. Detailed static pressure distributions on the blade surfaces were also recorded at a number of radial locations.

The general characteristics for the cascade at the nominal operating point are summarised in Table 1. Near the tip clearance region the inlet flow angle is $\sim 60^\circ$ from the axial direction, and the Mach number is of the order of 0.60 in the vicinity of the tip gap.

The effect of two different tip gap sizes (with rotating and stationary hubs) has been studied (2mm and 4mm) which correspond to 'clearance/chord' ratios of 2% and 4%, along with a zero tip gap, non-rotating condition.

Table 1. Summary of the cascade characteristics

Tip clearance (t/c)	2% and 4%
Pitch/chord ratio (p/c)	1.10 at tip, 0.78 at hub
Max blade Thickness/Chord	4.5%
Aspect ratio (h/c)	0.8
Chord (mm)	100
Span (mm)	80
Hub radius	0244m
Stagger (deg.)	51.4°
Number of blades	19
Hub rotational speed (rpm)	6500
Max. inlet Mach number	0.60
Inlet flow angle from axial	60° at hub
Design flow turning	10°
Reynolds number	1.1×10^6

A description of the flow physics is given by Bonhomme and Gerolymos [2], however the main aspects of the flow are highlighted here. There are three vortical structures of importance in the flow to be considered, and these are illustrated schematically in Figure 3 (Bonhomme and Gerolymos) [2]:

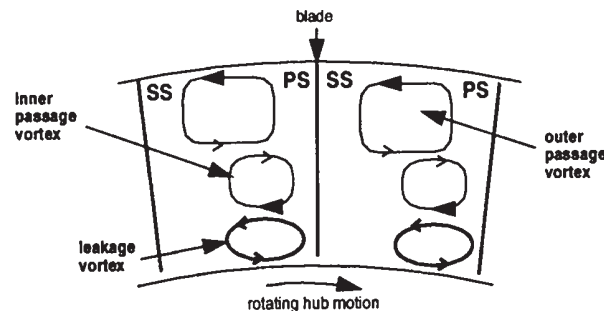


Figure 3. Schematic showing the vortical structures in the flow at 78% axial chord from the leading edge

Fluid from the clearance gap interacts with the main flow. High shear stresses exist near the tip gap exit due to the difference in flow direction between the main flow and the leakage jet, resulting in the formation of a discrete leakage vortex, called the tip-clearance vortex, which detaches from the blade suction surface causing a minimum in pressure there. The rotation of the hub carries this vortex to the pressure side of the next blade. The relative motion of the hub results in large flow under-turning at the wall. A strong interaction occurs between the leakage vortex and the wake immediately downstream of

the trailing edge, which rapidly dissipates the leakage vortex and increases losses. An inner passage vortex also exists, and this becomes displaced by the presence of the leakage vortex.

An outer passage vortex close to the casing turns from the pressure to the suction side of the wall. This vortex does not mix with the leakage vortex, and its trajectory is affected only slightly by the leakage vortex. The passage vortex dissipates much slower than the leakage vortex downstream of the trailing edge.

The size of the tip gap region strongly affects the flow. The location of the vortex initiation moves downstream as the tip gap height increases. This delay in formation is reflected in the shift of the static pressure trough on the blade suction side near the tip. Flow under-turning at the wall, and the total pressure losses are increased as the tip gap increases. The larger tip gap leads to a higher flow deficit at the hub, increasing the throughflow in the core flow region. This radial redistribution of the flow results in a lower static pressure, *i.e.* the annulus blockage effect.

Computations on this test case were performed by 4 partners. The codes, turbulence models, and the grids used by each of these partners are summarised in Table 2. A range of test configurations were considered, allowing the effects of different tip gap sizes (with rotating and stationary hubs) to be investigated, along with a zero tip gap, non-rotating condition. From an industrial perspective, the 2mm tip gap with a rotating hub was of greatest interest and was hence studied in most detail.

Table 2. Code information for the NTUA annular cascade

Partner name and CFD code	Model Equation Approach	Turbulence Model	Grid type
LEMFI/ UMPC TURBO 3D	3D/RANS Time marching	1. Launder-Sharma (1974) near wall $k-\varepsilon$ model [3] 2. Craft-Launder-Suga (1996) non-linear $k-\varepsilon$ model [4]	Three blocks – upstream and downstream structured ‘H’ grids, and 3 ‘O’ type mesh domains round blade, tip clearance region, and overlap
NTUA ELISA	3D/RANS Pressure correction	High Re. Number (Jones and Launder, 1972) $k-\varepsilon$ model [5]	Multi-domain approach using structured ‘H’ grids
SNECMA CANARI	3D/RANS Time marching	Mixing length model	O-type grid surrounding the blade, non-overlapping H-type grid for the tip gap
SNECMA TURBO 3D	3D/RANS Time marching	Linear $k-\varepsilon$ model	As above
VUB EURANUS/Turbo	3D/RANS Time marching	1. Baldwin and Lomax (1978) model [6] 2. Yang and Shih (1993) linear $k-\varepsilon$ model [7]	‘I’ type with non-matching periodic boundaries inside the blade passage

The effects of the tip leakage vortex predicted by CFD are demonstrated in the results shown in Figures 4 and 5. Figure 4 shows the yaw angle and pressure loss coefficient at plane 9 for the case of no tip gap, and no rotation. Figure 5 shows the same parameters with a 2mm gap, and no hub rotation. The experimental results show a reduction in the under-turning, whilst the computations predict an increase. The pressure coefficient plots show that the losses increase with the leakage flow, however the experiment shows only

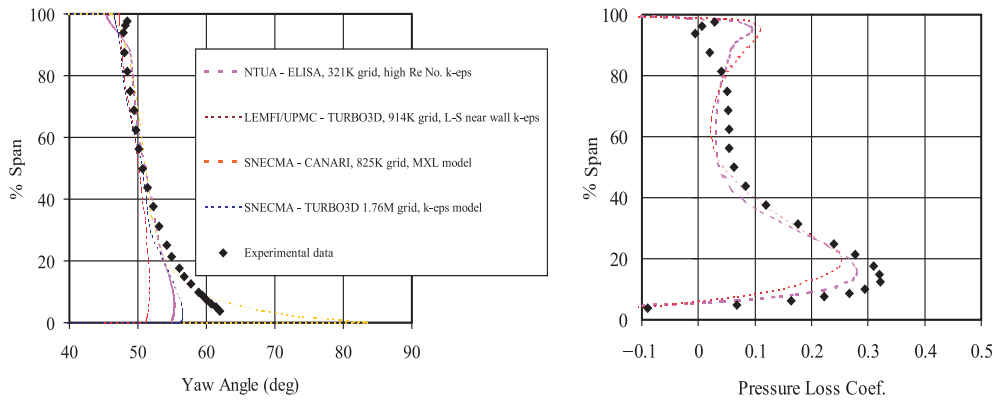


Figure 4. Pitch-averaged yaw angle and pressure loss coefficient at plane 9 for 0mm tip gap, no hub rotation

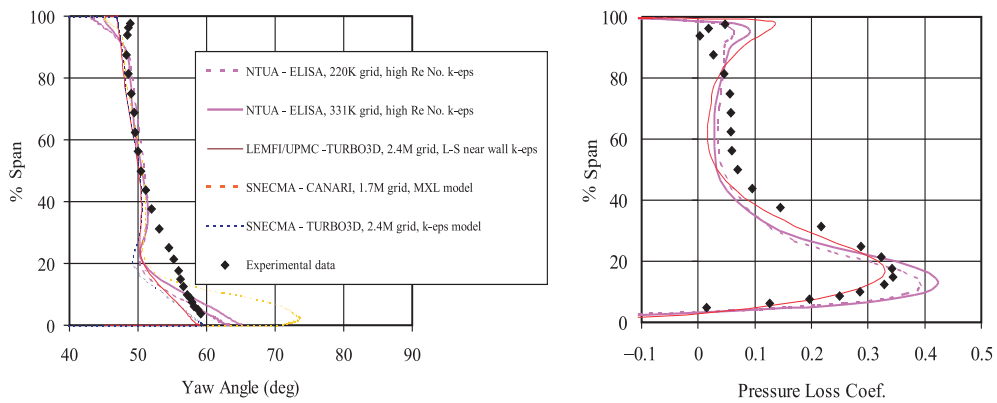


Figure 5. Pitch-averaged yaw angle and pressure loss coefficient at plane 9 for 2mm tip gap, no hub rotation

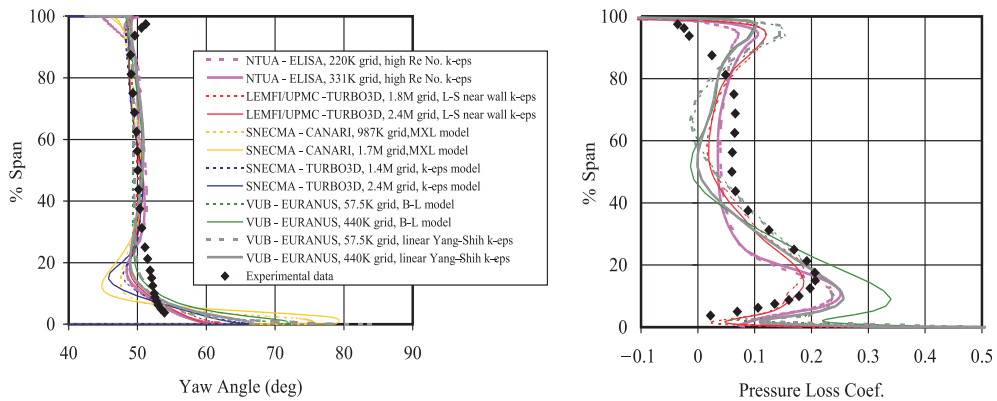


Figure 6. Pitch-averaged yaw angle and pressure loss coefficient at plane 9 for 2mm tip gap, hub rotating

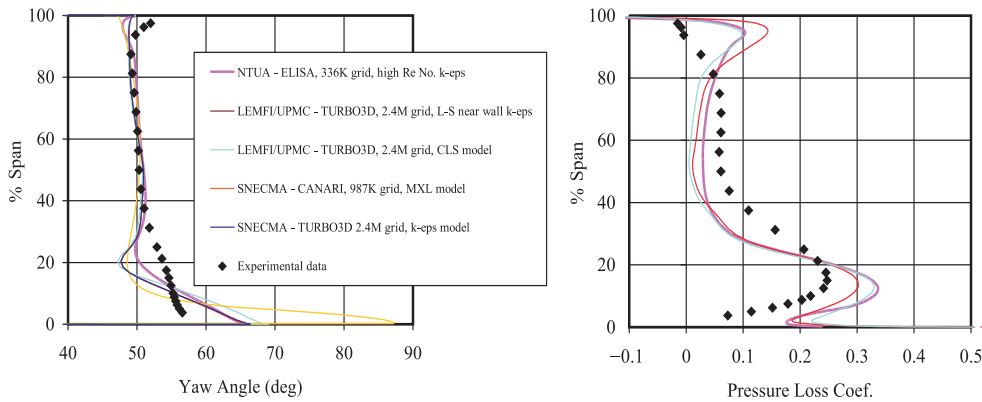


Figure 7. Pitch-averaged yaw angle and pressure loss coefficient at plane 9 for 4mm tip gap, hub rotating

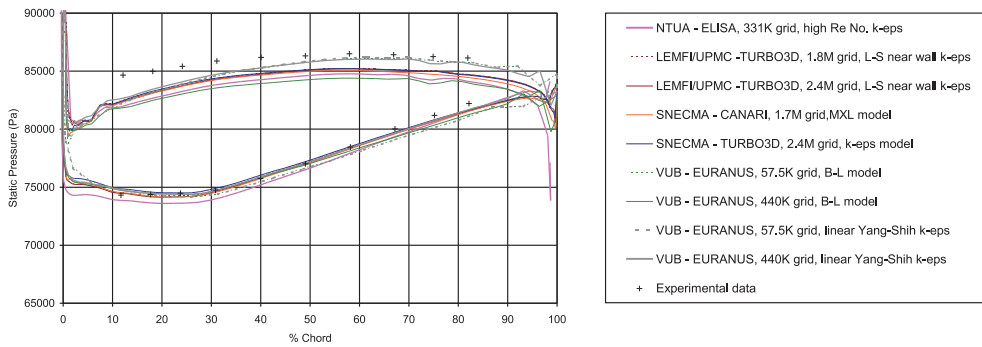


Figure 8. Blade surface static pressures at 41 mm above the hub for the NTUA cascade

a slight increase in loss. Figure 6 shows the yaw angle and pressure loss coefficient at plane 9 with a 2mm tip gap, with the hub rotating. The under-turning is clearly increased by the hub rotation in the computational results, but not in the experiment. One further point to be noted is that the losses are lower with a stationary hub. Figure 7 shows the results with twice the tip gap size, demonstrating that the losses do increase with the gap size, however this is more pronounced in the computations than in the experiments. The experimental data suggests that the tip-clearance vortex is completely mixed out by plane 9, yet the computations all under-predict the mixing, so evidence of the vortex still exists.

The computations were found to be successful in general at predicting the shape of the blade static pressure distributions, as illustrated in Figure 8, which shows the CFD results at 41 mm above the hub, where the experimental data is marked by crosses. Some discrepancies are apparent on the pressure side, but these may be due to experimental uncertainty.

4. NASA Rotor37

The NASA Rotor37 is an isolated axial flow compressor rotor which was designed and studied experimentally at the National Aeronautics and Space Administration Lewis Research Centre. Experimental data for this transonic rotor was obtained at various

measurement planes using LDV. Flow passage data based on radial surveys with pneumatic pressure probes and thermocouples also exists.

The Rotor37 was designed as an inlet stage for an eight stage 20:1 pressure ratio advanced core compressor for an aircraft engine. The ASME sponsored CFD assessment tested the rotor in isolation to avoid interactions between upstream inlet guide vanes or downstream stator blades. The design pressure ratio is 2106 at a mass flow of 20.19kg/s, with an inlet relative Mach number at the hub of 1.13 and 1.48 at the tip for a design tip speed of 454 m/s. The rotor aspect ratio is 1.19 and the hub/tip radius ratio is 0.70. The rotor has 36 blades with a nominal speed of 17,188 rpm, and a maximum mass flow at nominal speed, $m_{ch} = 20.93 \pm 0.14$ kg/s, with a nominal tip clearance of 0.356mm. A schematic of the rotor is shown in Figure 9. Under the APPACET project, only one operating point was investigated, defined as $m/m_{ch} = 0.9824$, where m_{ch} is the numerical choked mass flow.

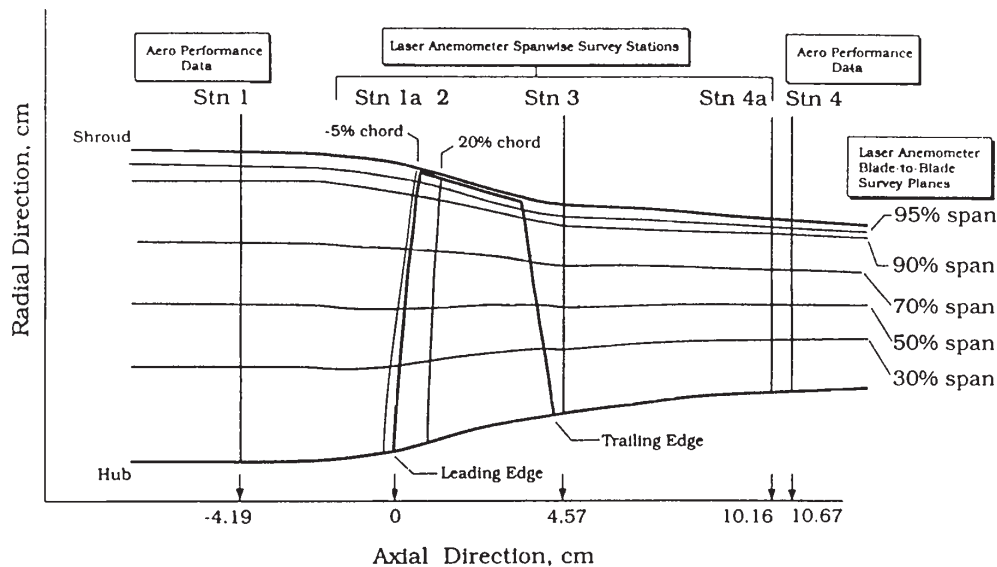


Figure 9. Schematic of the NASA Rotor37

A comprehensive description of the flow in the NASA Rotor37 is given in the AGARD Advisory Report 355 (1998) [8], however a brief description of the main flow regions is given below.

- A strong shock attached to the blade leading edge dominates the mid-span flow, which interacts strongly with the blade suction surface boundary layer. Following the impact of the shock wave, the boundary layer separates resulting in strong radial movement from the hub to the tip wall
- A region of low pressure at 20% of the blade span is apparent at station 4. Strazisar [9] notes this pressure deficit is present over a wide range of mass flows at the nominal speed of rotation. It is thought highly likely that a corner stall occurs near the suction side corner, which greatly reduces the axial momentum in the region of the stagnation pressure deficit near the hub. The axial momentum is then redistributed over the whole blade span, which reduces the work of the blade and hence the overall pressure ratio. The main influence on this corner stall is thought to be the supersonic Mach

Table 3. Code information for the NASA Rotor37 test case

Partner Code	Model Equation Approach	Turbulence Model	Grid type
UF TRAF3D	3D/RANS Time marching	1. Baldwin Lomax (1978) model [6] 2. MXL model (Arnone and Pacciani, 1996 [12])	Non-periodic C-type grids
UPMC TURBO-3D	3D/RANS Time marching	Launder-Sharma (1974) near-wall $k-\varepsilon$ model [3]	H-O-H grid for main flow and a fine grid for the tip clearance gap
VUB EURANUS/Turbo	3D/RANS Time marching	3. Baldwin and Lomax (1978) model [6] 4. Yang and Shih (1993) $k-\varepsilon$ model [7]	'I' grid with 3 structured blocks, 'H' grid in tip gap
DLR TRACE-S	3D/RANS Time marching	Standard $k-\varepsilon$ model, with wall functions	Structured, multi-block 'I' grid, 'H' grids up and downstream, and in tip gap, 'O' round blade
ALSTOM 3D-Denton	3D/Inviscid Euler solver	No turbulence model. Denton (1983) [13]	Structured 'H' grid generated using WHITTLE
Dawes' BTOB3D	3D/RANS Time marching	Baldwin and Lomax (1978) [6] algebraic model	
NEWT	3D/RANS Time marching	$k-\varepsilon$ model modified for low Re No. flows, Patel <i>et al.</i> , 1985 [14]	Solution adaptive unstructured grid
NTUA ATHENA	3D/RANS Time marching	Low Re no. $k-\varepsilon$ model [5] (Jones and Launder, 1972)	'H' type grid, blade pinched close to tip to accommodate tip clearance
ECL Proust	3D/RANS	$k-\omega$ model with constant turb. Pr No.=0.9	Structured 3D multi-block H-O-H mesh taking into account the tip clearance

number upstream of the leading edge, in the hub region, since lower subsonic Mach numbers upstream of the hub leading edge do not result in the pressure deficit (Shabbir *et al.* [10], Hah and Loellbach [11]). This corner stall may be partially caused by interaction of the glancing side wall shock wave with the hub boundary layer.

- The radial pressure distribution over the whole blade span is strongly modified by a change in the overall mass flow at a nominal speed. As the mass flow is reduced, the deficit in total temperature at the hub is always present, however the total pressure deficit becomes slightly smeared out at the higher mass flows.
- A leakage flow is believed to occur between the axial gap between the stationary upstream hub and the rotor. Experimental studies performed by Shabbir *et al.* [10] report an increase in the stagnation pressure downstream of the hub when the upstream axial gap is decreased. Most CFD simulations ignore the presence and effects of this upstream gap, and therefore over-predict the total pressure in the hub region, and all over the blade span.

The NASA Rotor37 shows other complex flow phenomena such as corner stall, shock-boundary layer, tip-vortex and tip leakage-secondary flow interactions. This test case also shows a strong interaction between the tip vortex and the leading edge shock, which largely controls the stall behaviour. All these interactions are challenging for any CFD simulation, and previous studies have shown the simulations are highly dependent on the mesh and turbulence modelling used. Under the APPACET project, 7 partners performed calculations

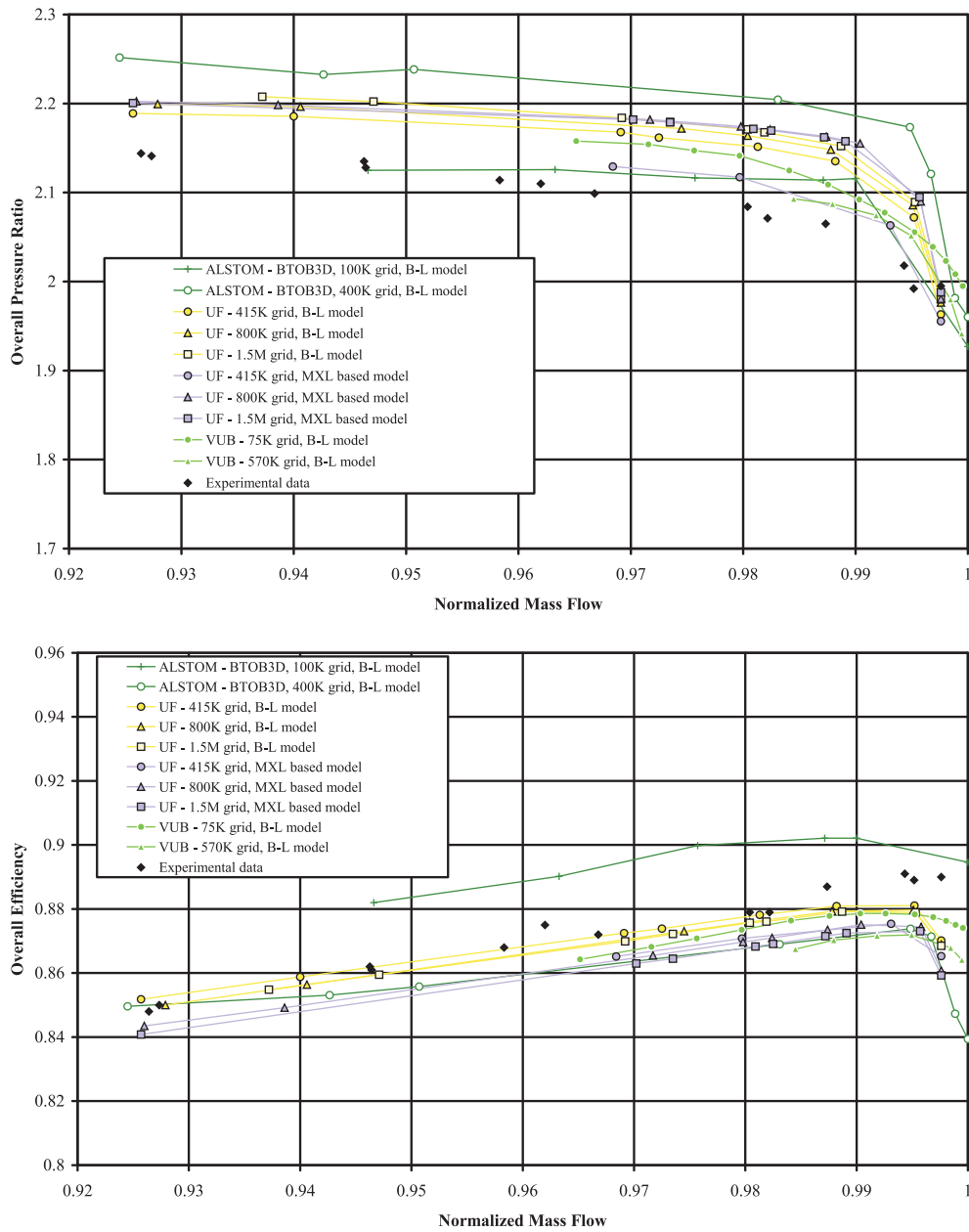


Figure 10. Operating maps computed using algebraic/mixing length models

on this test case. The partners involved, and the models used by each are summarised in Table 3.

Initial work by UF on this test case showed that the discretisation on the blade leading edge has a great impact on the total pressure ratio, so all partners were requested to use a minimum of 10 grid points in this region of their grid. The computational results were assessed in a number of ways, including operating maps of total pressure ratio and isentropic efficiency, and pitch-averaged radial distributions were computed for stations 3 and 4.

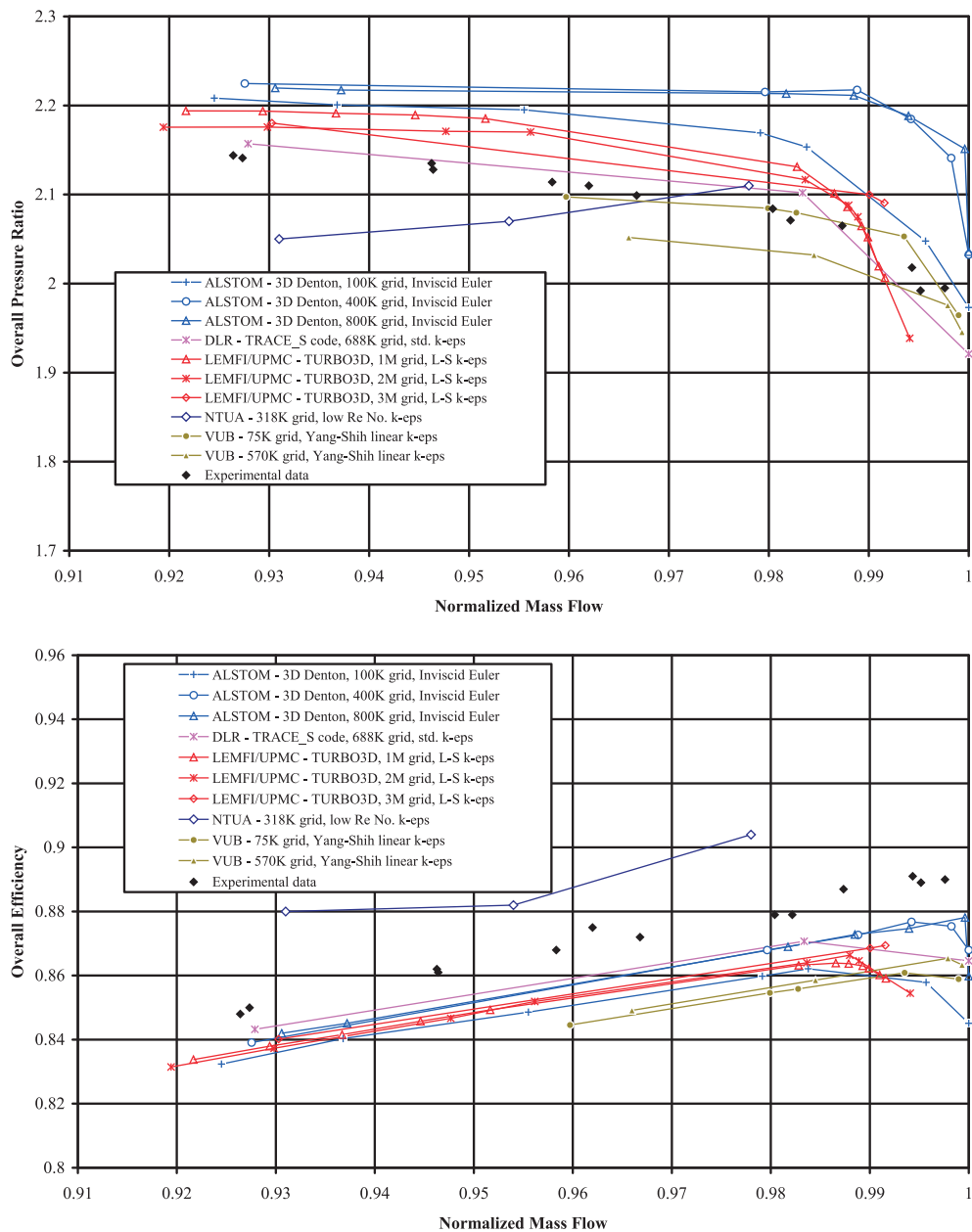


Figure 11. Operating maps computed using turbulent transport models

The operating maps produced by the algebraic/mixing length models are shown in Figure 10. These models tend to over-predict the pressure ratio, and under-predict the efficiency, and grid refinement increases the discrepancy between predicted and experimental results. The Baldwin Lomax model of ALSTOM appears to be the most sensitive to grid refinement. The operating maps for the turbulent transport models are shown in Figure 11, which shows grid refinement improves the pressure ratio and efficiency predictions. The majority of the models show a decrease in efficiency as the choked condition is approached,

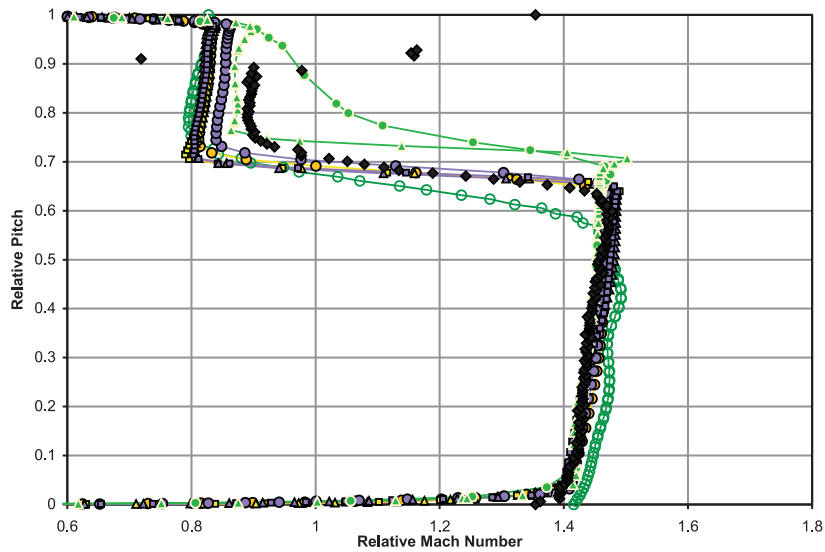


Figure 12. Relative Mach number plots at station 2 computed using algebraic/mixing length models (see Figure 10 for legend)

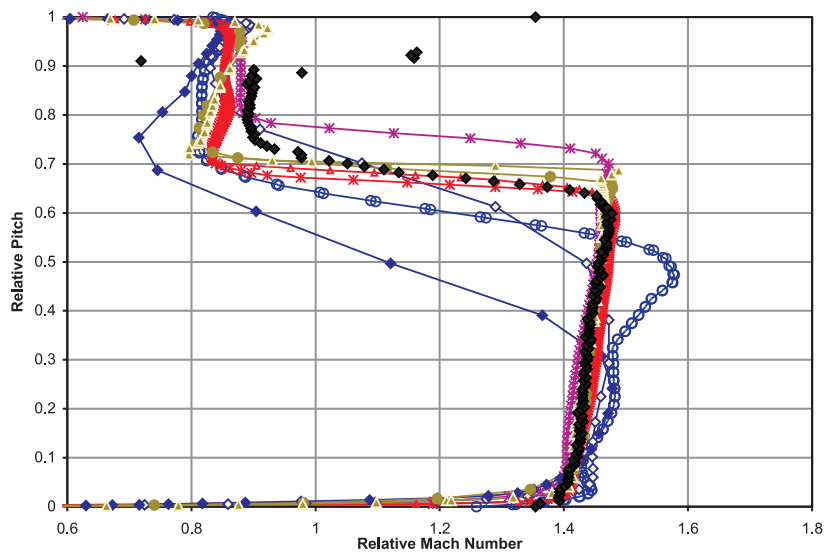


Figure 13. Relative Mach number plots at station 2 computed using turbulent transport models (see Figure 11 for legend)

in contrast to the experimental data. Nearly all the computations seem to under-predict the efficiency, however the algebraic/mixing length models appear to be closer to the experimental results.

Some features found that are not illustrated here were:

- Most models were found to be incapable of resolving the tip clearance gap flow correctly. All the models failed to predict the corner stall at station 4, and at station 3, only LEMFI/UPMC ($k-\epsilon$) and UF (MXL) predict the dip in total pressure near the hub, which resembles the experimental data.

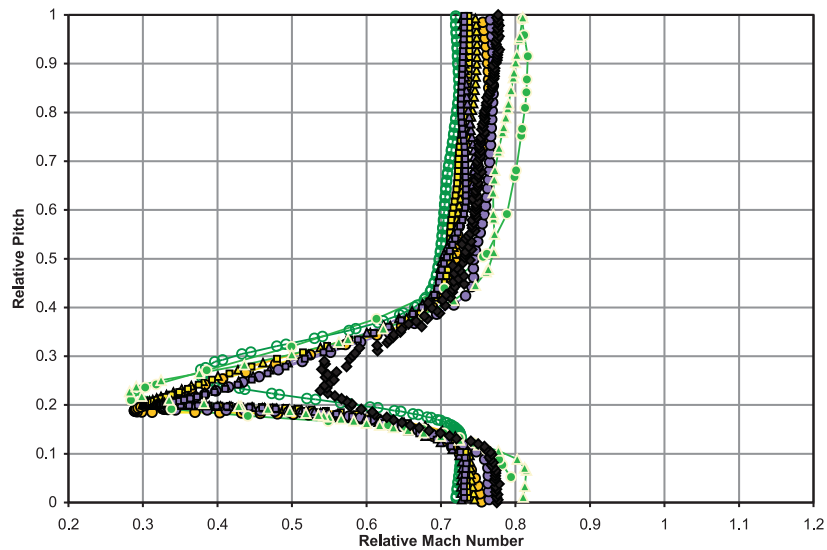


Figure 14. Relative Mach number plots at station 3 computed using algebraic/mixing length models (see Figure 10 for legend)

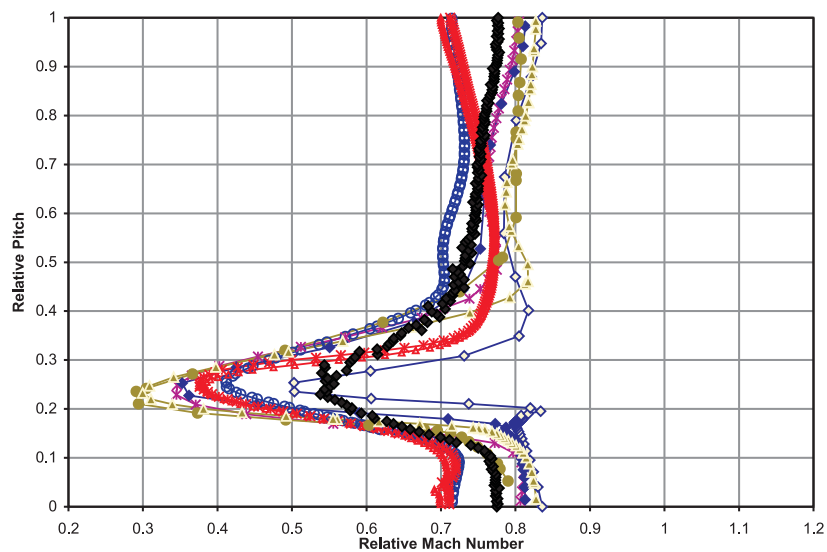


Figure 15. Relative Mach number plots at station 3 computed using turbulent transport models (see Figure 11 for legend)

- The radial distribution for the total temperature gives a good estimate for the axial velocity component, and hence the work done by the rotor. With the exception of NTUA ($k-\varepsilon$ model), all computations over-predict the total temperature, and hence over-estimate the work done by the rotor. This over-estimation is either due to an axial velocity which is too low, and/or a decrease in the relative flow angle. Pitch-averaged efficiency plots show that nearly all the models predict high losses near the tip wall, which should mean that the mid-span axial velocity increases, corresponding to a reduction in work. However, the total temperature ratio is generally not computed

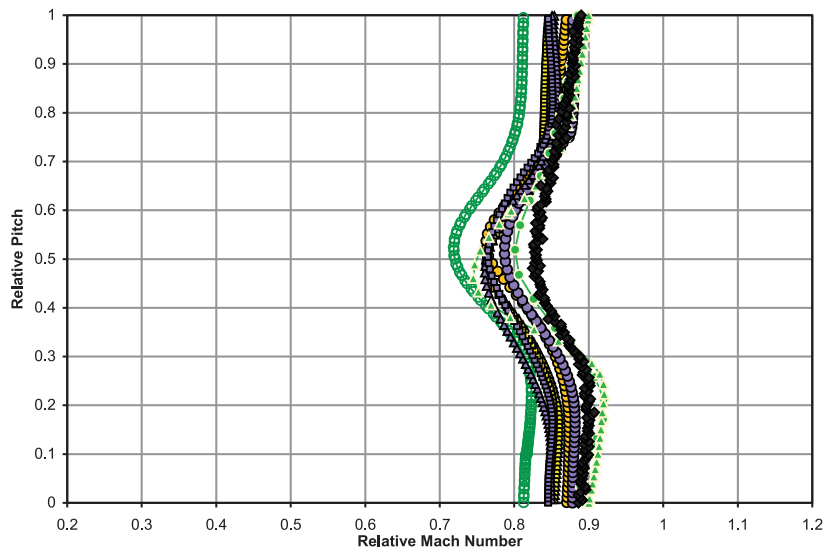


Figure 16. Relative Mach number plots at station 4a computed using algebraic/mixing length models (see Figure 10 for legend)

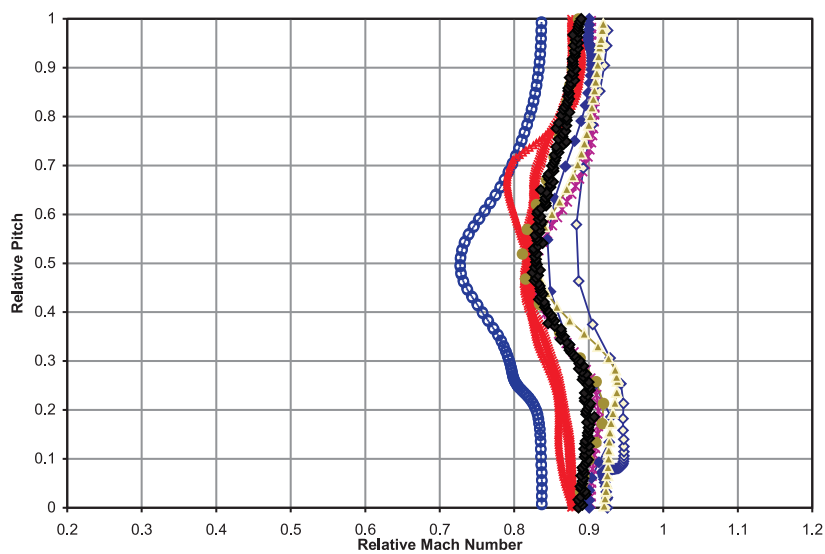


Figure 17. Relative Mach number plots at station 4a computed using turbulent transport models (see Figure 11 for legend)

to be lower at mid span, which may be due to the influence of error in the choked mass flow.

An examination of the relative mach number at station 2 shows that shock smearing is reduced by grid refinement, with LEMFI/UPMC ($k-\varepsilon$ model) capturing the position and strength of the shock most accurately. Plots of computed relative Mach number at 50% at station 2 are shown in Figure 12 and 13. All models showed the greatest disagreement with experimental data at 95% span. Downstream of the shock, all models predicted the Mach number to be lower than the experimental value, implying that the computed shocks

are too strong. Figure 14 and Figure 15 show the Relative Mach number plots at 50% for station 3, and Figure 16 and Figure 17 show results at station 4a. At station 3, the wakes are all deeper than the experimental one. With grid refinement, the algebraic models predict a decreased wake depth, whilst the turbulent transport models predict an increase. Between stations 3 and 4a, the models seem to over-predict the dissipation rate of the wake, but in general the turbulent transport models possibly perform better than the algebraic/mixing length models.

5. Contra-rotating fan

The first of the unsteady flow test cases was the contra-rotating fan CRISP (Counter-Rotating-Integrated-Shrouded-Propfan), designed by the German manufacturer MTU and tested by DLR, see [15–17]. The fan consists of two rotors which rotate in opposite directions, with 10 and 12 blades for the first and second rotors. The design has neither an inlet guide vane nor a stator behind the rotors. The mass flow and pressure rise were recorded, and Laser anemometry (using a Laser-2-Focus system) provided unsteady velocities and flow angles at inlet and exit from both rotors at a radius of 0.353 m (*i.e.* 2D data). This test case also provided data on blade row interactions with both wakes and shock waves. It considers a 2D plane at 60% span with stream-tube thickness variation specified from a quasi-steady 3D computation. The design data is summarised in Table 4. Three partners were involved in this test case, ALSTOM, DLR, and UF, and the codes used by each are summarised in Table 5.

Table 4. Propfan design data

Outer diameter	1 m
No. Blades rotor 1	10
No. Blades rotor 2	12
Rotational speed rotor 1 (design point)	−4980rpm
Rotational speed rotor 2 (design point)	4316rpm
Design mass flow (design point)	166kg/s
Design total pressure ratio (design point)	1242

ALSTOM performed a quasi-steady calculation using a mixing plane approach for the rotor/rotor-coupling. DLR and UF both solved the 2D Reynolds Averaged Navier Stokes (RANS) equations to perform full unsteady computations. DLR reduced the blade count to 5:6, and used a grid of 20K points. UF used the TRAF2D code, computing blade counts of 5:6 and 10:12, and reported no significant impact in reducing the blade count.

The time-averaged unsteady solutions obtained by DLR and UF were compared against each other, and the quasi-steady results of ALSTOM. Specific unsteady parameters were also considered, and comparisons made between the two unsteady solutions, and the experimental data. Firstly, comparisons were made between the overall characteristics of the operating point. Detailed comparisons were then made between the blade surface pressure distributions; the lift of both rotors, and its unsteady evolution; mass flow fluctuations at two axial positions. Finally comparisons were made between pitchwise distributions of velocity and flow angle at four axial stations, including time-averaged and fluctuating measurements.

Table 5. Code information for the CRISP fan

Partner (Code)	Model Equation Approach	Turbulence Model	Grid type	Space/Time discretisation and convergence acceleration
ALSTOM (3D-Denton)	3D/Euler time marching, (body force terms to simulate viscous effects)	—	Structured H-grid	Steady: Finite volume, explicit time integration. Mixing plane for rotor/rotor coupling
DLR (TRACE-U)	2D/RANS time marching (source terms for variable streamtube height)	Spalart-Allmaras 1-equation model	Structured H-O-H-grid	Unsteady: Finite volume, upwind, four stage Runge-Kutta time integration with time-consistent two-grid
UF (TRAF2D)	2D/RANS time marching, (source terms for variable streamtube height)	Algebraic Baldwin-Lomax model [6]	Structured H-grid	Unsteady: Finite volume, centered, dual time stepping, fully implicit outer time integration, 4 stage Runge-Kutta inner time integration with local time stepping, residual smoothing and multi-grid

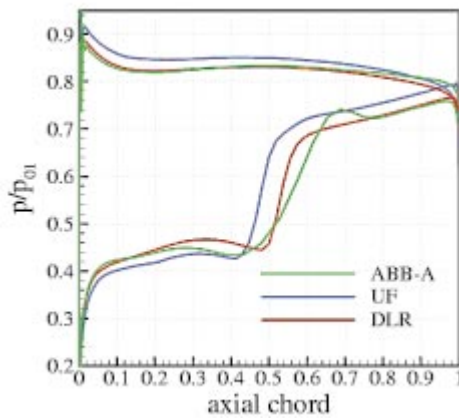


Figure 18. Blade surface pressures for rotor I

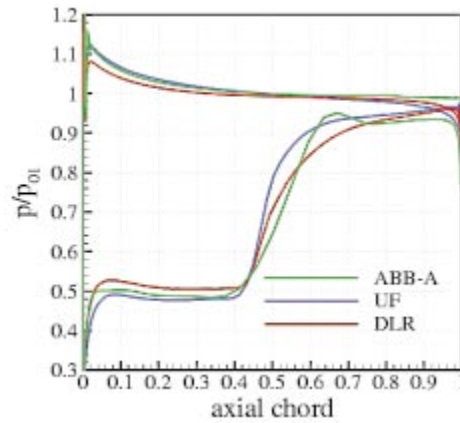


Figure 19. Blade surface pressures for rotor II

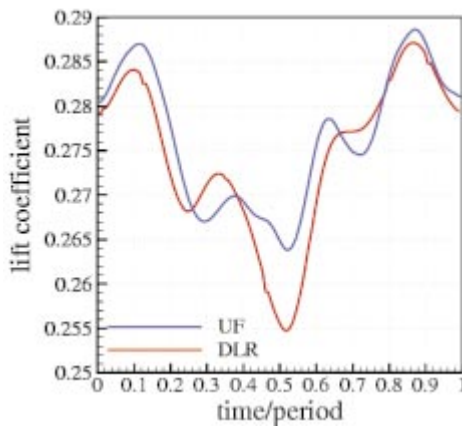


Figure 20. Time evolution of rotor II lift

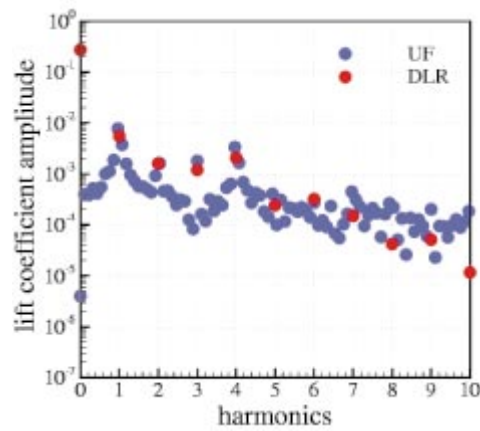


Figure 21. Harmonic spectrum of rotor II lift

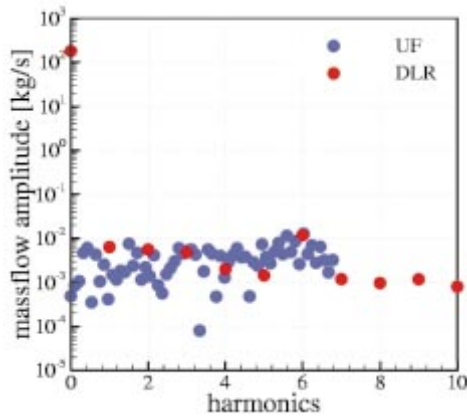


Figure 22. Harmonic spectrum of mass flow between the rotors

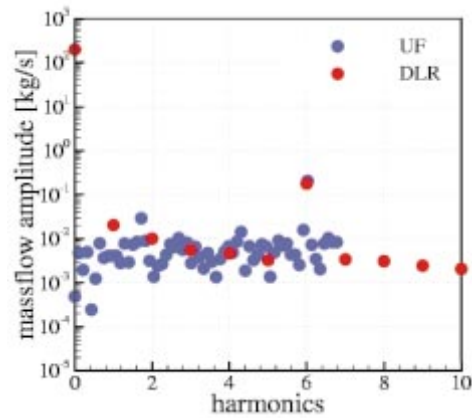


Figure 23. Harmonic spectrum of mass flow at exit

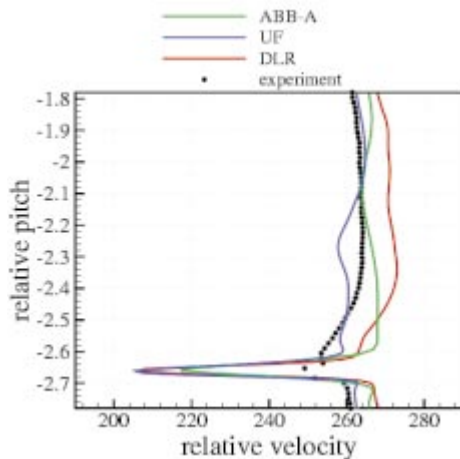


Figure 24. Pitchwise distribution of relative velocity downstream of rotor I

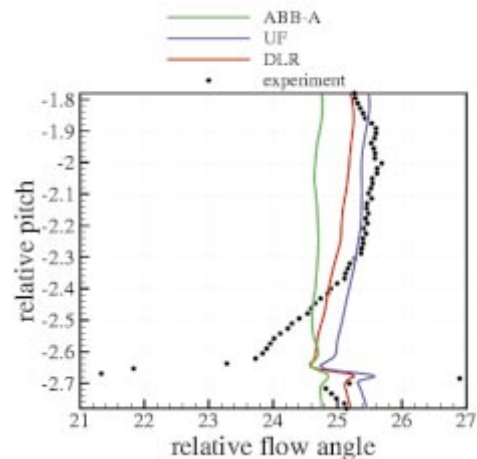


Figure 25. Pitchwise distribution of flow angle downstream of rotor I

The type of turbulence model used may have an effect on the operating point predicted, since DLR calculate a higher mass flow and total pressure ratio than UF, which may be due to the different turbulence models predicting different boundary layer thicknesses, resulting in different blade blockages and hence slightly different incidence angles for the rotors and different predictions for flow turning. In future work it is suggested that the total pressure ratio should be specified instead of the static outlet pressure, or that the operating point should be specified in relation to the choked mass flow rate, which could lead to a better agreement in operating point and hence a better basis for detailed flow comparisons.

Time-averaged plots of blade surface pressure distributions, shown in Figures 18 and 19, reveal that all three simulations predict different pressure distributions and shock positions, which reflects the different operating points and incidence angles calculated by the simulations. ALSTOM predict an overshoot near the shock location on both rotors, which could be an effect of using the H-type of mesh. DLR predicts a weaker shock than UF on rotor 1, which is also located further downstream, which could be due to the difference in turbulence models, predicting a thinner boundary layer for DLR. The unsteady

calculations of DLR and UF showed good qualitative agreement for the unsteady surface pressure fluctuation amplitudes, with both codes predicting higher fluctuations at the rotor 1 trailing edge due to the upstream running shock from rotor 2, and similar (higher) fluctuation levels on rotor 2 that slowly decayed towards the trailing edge.

The harmonic spectrum for the lift coefficient of each rotor was examined for the two unsteady computations. The computations were found to be in good agreement with each other, both predicting a high contribution of the 4th harmonic to the lift of the second rotor, as illustrated in Figures 20 and 21. The source of this harmonic is the reflection of the rotor 2 shock at the rotor 1 trailing edge. The prediction of this complicated interaction mechanism in qualitative and quantitative terms proves the ability of both unsteady codes to provide a detailed investigation of blade row interaction phenomena.

The unsteady calculations also gave good agreement for the harmonic spectrum for the total mass flow, predicting very low fluctuation levels. The harmonic spectra for the mass flow between the rotors, and at the exit, are shown in Figure 22 and Figure 23, respectively. Both DLR and UF predicted the influence of a 6th harmonic at the exit from the second rotor, which can be linked to the most important wave of rotor 2.

Pitchwise velocity and flow angle distributions provided a detailed assessment of the performance of all three calculations. The pitchwise distributions of relative velocity and flow angle downstream of rotor I are shown in Figures 24 and 25, respectively. These time-averaged unsteady and the steady flow features generally are all in good agreement with each other, and the experimental data. All predict slightly stronger pitchwise variations across the shocks, either due to the forced propagation of the waves on a constant radius due to the 2D approach of the simulations, or the slight differences in operating points. The greatest discrepancy between computations and experimental data is observed in the velocity distribution near the trailing edge of rotor 2. This discrepancy is localised in nature, and once more attributable to the 2D nature of the simulations, or differences in operating point.

The fluctuation amplitudes of pitchwise velocity and flow angle of both unsteady simulations were in qualitative and quantitative agreement with the experimental data. Pitchwise variations observed in the simulations and experiment were found to be caused by the local impact of a velocity and flow angle perturbation on the local velocity vector.

To summarise, the quasi-steady computation of ALSTOM, and the unsteady computations of DLR and UF, all successfully reproduced the general flow features of the propfan flow. The extent of the agreement between computations and the experimental data appears to be governed in part by the turbulence model used, since this appears to influence the calculated operating point. A second factor which could limit the agreement is the method of using a variable streamtube height on a constant radius in order to model the 3-dimensional effects. Finally, transferring the operating point for the experiment to a numerical one for the simulations may be a further limiting factor.

6. Aachen 1–1/2 stage turbine

The Aachen turbine, illustrated in Figure 26, comprises of a stator, rotor and stator, operating in an axial configuration at modest Mach numbers of ~ 0.5 . Experimental data for this test case existed for two operating points, corresponding to experimental mass flows of 8.02 kg/s and 6.7 kg/s. The low aspect ratio of the blades, and the constant tip and

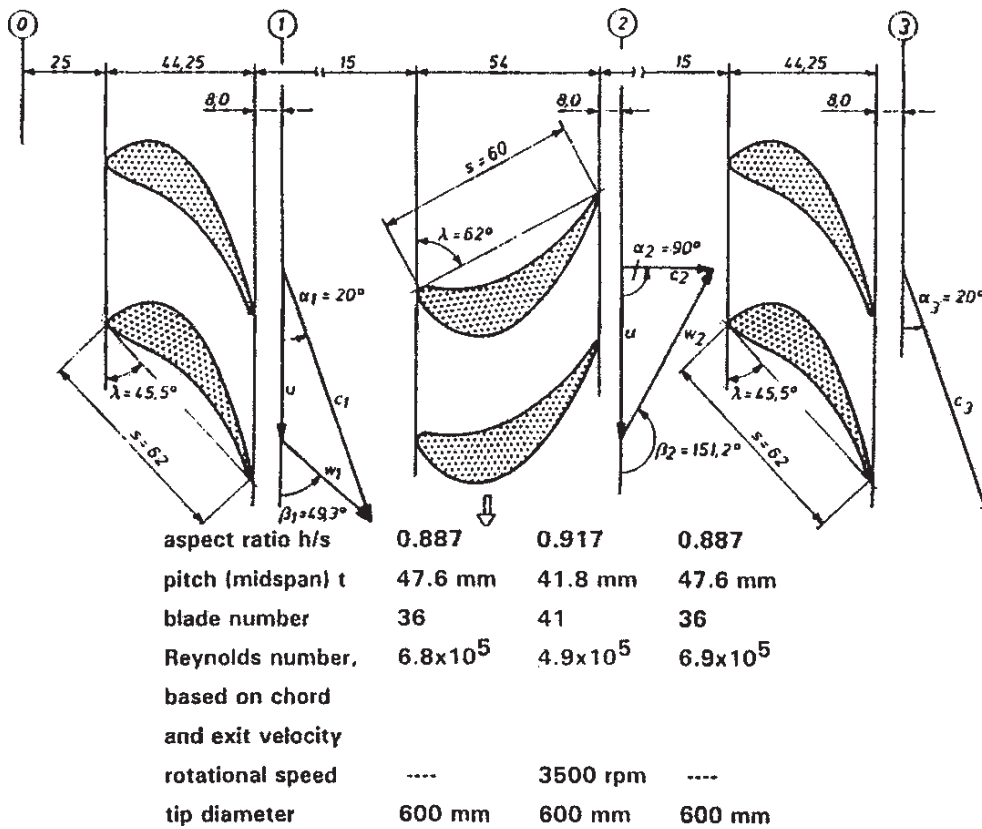


Figure 26. Schematic of the Aachen turbine rig, showing the positions of the measuring stations

hub endwall contours enhance strong secondary flow phenomena. Both the 36 vanes and 41 blades are cylindrical and untwisted. The rotor is unshrouded with a tip clearance of 0.4 mm. Experimental measurements were performed at four axial locations. Steady measurements were obtained using a five hole probe between 10–90% span, and a three hole probe near the endwalls. Unsteady data was obtained at 64 different rotor positions distributed along one rotor pitch using a triple hot wire. The unsteady rotor exit absolute flow angle and the relative Mach number were used for comparisons with CFD computations.

The steady-state multistage calculations were performed using mixing planes at the interfaces of each row, where pitchwise averaging was applied to the solution before transferring the flow quantities from one block to another. Unsteady calculations were performed using a technique known as the Domain Scaling Method, which involves changing the pitch/chord ratio of the rotor to make the blade count 1 : 1 (originally 36 : 41), which results in a change in the blade loading.

Four partners were involved with this test case – ALSTOM, Fiat Avio, LEMFI/UPMC, and VUB. Fiat Avio used the flow solver TRAF3D with the Baldwin Lomax turbulence model. Quasi-steady calculations were performed for the two operating points. The effects of spanwise grid refinement were studied for the higher mass flow operating point, with 40, 80 and finally 120 cells in the radial main flow region, corresponding to a total number of

600K, 1.2M and 1.8M grid cells, respectively. Original calculations using the coarsest grid illustrated the solution's inability to capture the behaviour of the secondary and tip clearance flows in the turbine. As the grid was refined the losses were found to increase, however the difference between the 80 and 120 radial cells was significantly less than the difference between the grids with 40 and 80 radial cells. Fiat Avio concluded from this that 80 cells in the radial direction, and 12 within the clearance gap, should be sufficient to understand the tip-clearance losses. Fiat Avio performed a full unsteady computation for the higher mass flow rate operating point, using the Domain Scaling Method which reduces the blading ratio to 1 : 1 by increasing the number of stator blades from 36 to 41, whilst maintaining the stator blade geometry. The intermediate grid with 80 cells in the radial direction was used for this unsteady computation. The unsteady time-averaged computation has been compared against the steady state result, which illustrated a large discrepancy in the computed mass flows, largely due to the different geometries used in the two computations. To address this problem, Fiat Avio repeated the steady calculations using the scaled geometry and found good agreement between the two calculated mass flow rates, both of which were $\sim 7.5\%$ lower than the experimental value. The unsteady time-averaged solution was found to be very close to the steady state one obtained on the scaled geometry, suggesting that the time-averaged unsteadiness has only a minor impact on the stationary features of the flow field. The unsteady and steady-state calculations performed on the scaled geometry seem to be unable to capture the passage and tip-clearance vortices correctly, unlike the steady state analyses performed on the unscaled geometry.

VUB used the EURANUS/Turbo flow solver with the Baldwin Lomax turbulence model. Three I-type structured blocks were used for the mesh, with a total of 940K grid points, with only one blade passage per row discretised, and 97 grid points in the radial direction in the main flow path. Four different calculations were performed – two quasi-steady calculations at the two operating points using the real stage geometry, and a third quasi-steady calculation for the higher mass flow, but using the scaled geometry, in order to investigate the effect of grid scaling on the accuracy of the flow solution. The final calculation they performed was an unsteady calculation at the high mass flow rate, using the scaled geometry.

VUB made comparisons between the quasi-steady solutions obtained on the real and scaled geometries, and found that for all measuring stations the pitch-averaged data computed on the scaled geometry was in better agreement with the experimental data, suggesting that grid scaling does not reduce the accuracy of the flow solution at the quasi-steady level of approximation. Two effects of grid scaling that VUB observe are that for a given mass flow rate, the computed total pressure ratio of the turbine is reduced, and since the pitch to chord ratio changes due to scaling, the secondary flows are affected, which changes the radial position of the hub corner vortex from $\sim 40\%$ on the real geometry, to $\sim 50\%$ on the scaled geometry. The time-averaged unsteady solution obtained on the scaled geometry gave good agreement with the experimental data, showing that the unsteadiness of the flow field does not affect the accuracy of the computed flow solution when compared against the data from quasi-steady calculations. At plane 2 the quasi-steady and full unsteady solutions are in good agreement with the experimental data, mainly due to the small variation in time of the absolute flow angle at station 2. However, at station 3 the unsteadiness of the flow field plays a more important role, and the unsteady data was found to be in better agreement with the experimental data.

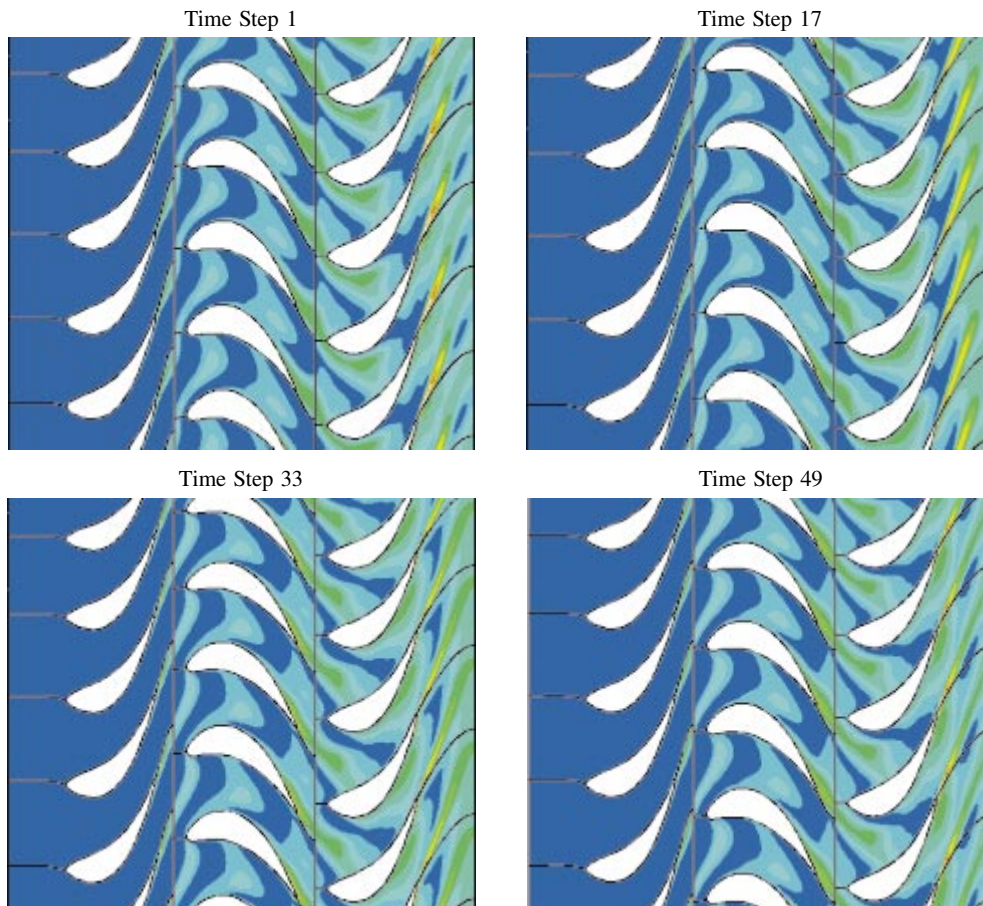


Figure 27. Entropy contours computed by VUB at mid-span for the Aachen Turbine

In the unsteady computations, the first wake cutting by the rotor blade and the subsequent second stator wake cutting were observed, and this is illustrated in the series of entropy contours shown in Figure 27.

LEMFI/UPMC used the Gerolymos-Vallet [18] near wall RSM turbulence model on an H-O-H grid for the main flow, with a total of 4.5M grid points, with 121 radial stations in the main flow path. They report that previous studies have shown that the y^+ value needs to be less than 0.75 in order to obtain grid independency in transonic flow conditions. LEMFI/UPMC performed two calculations – both at the high mass flow operating point. The first was a steady computation, and the second an unsteady computation initialised from the steady flow solution.

The differences that UPMC observe between the steady and unsteady results differ from those of VUB and Fiat Avio (which both use the Baldwin Lomax model). These differences are illustrated in Table 6, which compares the differences between steady and unsteady results obtained by each partner. Firstly, UPMC predict a 0.5% higher mass flow with the unsteady computation, whereas the others predict a lower mass flow rate. Their predictions for efficiency are also higher with the unsteady computation, whereas they predict a lower efficiency than obtained with the steady solution. Despite these differences,

their overall conclusions are the same, namely that the unsteady and steady solutions give good results, and that the unsteady calculation shows no major improvement over the steady calculation for predicting the time-averaged flow quantities.

ALSTOM used the 3D Denton code which solves the Euler equations and uses body forces to represent the losses. Calculations were performed on a straight H mesh with 706K points, with 49 in the radial direction. A quasi-steady solution was obtained for the lower mass flow rate operating point. The overall mass flow rate was over-predicted by this code, however the overall pressure ratio was predicted to be close to the experimental value. In general the Denton code was found to give reasonable agreement with the experimental measurements. The code predicted the level of total pressure distribution well for stator 1 and stator 2, however it failed to accurately predict the total pressure losses near the endwalls due to the secondary flows.

Table 6. Overall results for the quasi-steady and fully unsteady computations by the three partners

Partner	Parameter	Measured	Steady (real geo.)	Steady (scaled geo.)	Unsteady (scaled geo.)
Fiat Avio	Mass flow (kg/s)	8.02	8.26	7.62	7.62
	p_{t1}/p_{t0} – stator 1	0.9934	0.9919	0.9915	0.9906
	p_{t3}/p_{t2} – stator 2	0.9862	0.9866	0.9858	0.9864
	p_{t0}/p_{t2} – stator 1 + rotor	1.1879	1.1715	1.1728	1.1721
	p_{t0}/p_{t3} – stator 1 + rotor + stator 2	1.2007	1.1876	1.1901	1.1887
	Stage efficiency (stator/rotor) [%]	—	89.15	89.24	88.69
	Overall efficiency (stator/rotor/stator) [%]	—	82.15	81.67	81.13
VUB	Mass flow (kg/s)	8.02	8.396	8.385	8.363
	p_{t1}/p_{t0} – stator 1	0.9934	0.9929	0.9905	0.9902
	p_{t3}/p_{t2} – stator 2	0.9862	0.9875	0.9857	0.9852
	p_{t0}/p_{t2} – stator 1 + rotor	1.1879	1.1804	1.2061	1.2042
	p_{t0}/p_{t3} – stator 1 + rotor + stator 2	1.2007	1.1953	1.2235	1.2220
	Stage efficiency (stator/rotor) [%]	—	91.22	90.47	89.36
	Overall efficiency (stator/rotor/stator) [%]	—	84.99	84.24	84.11
UPMC	Mass flow (kg/s)	8.02	—	8.2514	8.2951
	p_{t1}/p_{t0} – stator 1	0.9934	—	0.9931	0.9945
	p_{t3}/p_{t2} – stator 2	0.9862	—	0.9897	0.9909
	p_{t0}/p_{t2} – stator 1 + rotor	1.1879	—	1.1810	1.1802
	p_{t0}/p_{t3} – stator 1 + rotor + stator 2	1.2007	—	1.1939	1.1914
	Stage efficiency (stator/rotor) [%]	—	—	91.76	92.01
	Overall efficiency (stator/rotor/stator) [%]	—	—	86.65	87.58

7. Conclusions

The major objectives of the APPACET project were the understanding, evaluation and modelling of the main unsteady loss sources in rotor/stator interactions. This was achieved through new advanced experimental data coupled to systematic and controlled numerical

simulations, at the full unsteady and quasi-steady levels of approximation, with the object of providing the designer with modelling guidelines. Unsteady phenomena are dependent on turbulent and eventually transition effects, but it is not considered feasible, at the present level of flow modelling, to assess the validity of turbulence models on unsteady data. Therefore, this effort was performed on steady simulations of test cases representative of the complex 3D flow structure of advanced compressors.

Two important conclusions of the results of the computational comparisons are:

- Two steady flow test cases have been investigated, namely the transonic NASA Rotor37 and the NTUA annular cascade. These involve some important flow features such as corner stall, shock-boundary layers, tip vortex and tip leakage secondary interactions. The importance of grid refinement has been clearly demonstrated, independently from the used grid topology. Some necessary requirements to capture the basic flow features were also highlighted. However, no evidence was found that one family of turbulence models could be definitely better than the other.
- The two unsteady Test Cases, 4 (the DLR counter rotating fan) and 5 (the 1–1/2 axial turbine stage from Aachen) have been investigated numerically using both the quasi-steady and fully unsteady levels of approximation. Compared to steady results, unsteady time-averaged solutions have not shown any major improvement in accuracy. However many unsteady flow phenomena generating losses within each blade row have been captured and partly explained. Conclusions have been used to derive modelling guidelines.

CFD is nowadays a common tool in the design process of industrial turbomachinery applications. It has been recognised however that even if CFD may now be seen as mature, many questions still remain open: What are the effects of grid refinement and of turbulence modelling on the accuracy of the computed flow field for complex turbomachinery configurations, such as those where tip-clearance secondary flows play a major role? How can we trust results obtained from CFD for state-of-the-art problems such as unsteady rotor/stator interactions? The APPACET project has helped to answer these questions by comparing computational results obtained using different codes, grids and turbulence models, and through exchange of expertise between industrial and university partners. Synthesis of results and recommendations obtained as part of this project are then extremely valuable. They will benefit the European CFD community through improvements of the different partner's codes, and through the presentation of experimental and calculation results in the database and in publications. Some of the data and results of computations can be found on the web site: <http://www.dur.ac.uk/APPACET/> and some publications from the project are listed below:

Aubé M and Hirsch Ch, June 2001, *On the Numerical Investigations of the 1–1/2 Axial Turbine Stage from Aachen at Both Quasi-Steady and Fully Unsteady Levels of Approximation* Abstract to the 46th ASME International Gas Turbine and Aero-engine Technical Congress, Exposition and Users Symposium, New Orleans, Louisiana, USA

Oliveira G, March 1999, *Analyse numérique de l'effet de défilement des sillages liés aux interactions rotor/stator en turbomachines* Thèse de doctorat, Ecole Centrale de Lyon

Oliveira G, Ferrand P and Aubert S, 18–23 July 1999, *Inlet Wakes Influence on Axial Transonic Compressor Performance's* 3rd ASME-JSME joint Fluids Engineering conference, San Francisco

Ottavy X, 10 May 1999, *Mesures par Anémométrie Laser dans un compresseur axial transsonique. Etude des structures instationnaires périodiques* Thèse de doctorat, Ecole Centrale de Lyon

Ottavy X, Trébinjac I and Vouillarmet A, 8–11 May 2000, *Analysis of the Inter-row Flow Field within a Transonic Axial Compressor: Part I – Experimental Investigation* ASME Paper 2000-GT-0496, Munich

Ottavy X, Trébinjac I and Vouillarmet A, 8–11 May 2000, *Analysis of the Inter-row Flow Field within a Transonic Axial Compressor: Part II – Unsteady Flow Analysis* ASME Paper 2000-GT-0497, Munich

Schmitt S, Eulitz F, Arnone A and Marconcini M, June 2001, *Evaluation of Unsteady CFD Methods by their Application to a Transonic Propfan Stage* Abstract to the 46th ASME International Gas Turbine and Aero-engine Technical Congress, Exposition and Users Symposium, New Orleans, Louisiana, USA

Acknowledgements

The authors acknowledge with grateful thanks all the computations performed by the other APPACET partners, and also the financial support of the European Community.

References

- [1] Mathioudakis K, Papailliou K, Neris N, Bonhommet C, Albrand G and Wenger U 1997 *An Annular Cascade Facility for Studying Tip-clearance Effects in High Speed Flows* XIII ISOABE Chattanooga
- [2] Bonhommet-Chabanel C and Gerolymos G A 1998 *Analysis of Tip Leakage Effects in a High Subsonic Annular Compressor Cascade* ASME Paper 98-GT-195
- [3] Launder B E and Sharma B I 1974 *Letters in Heat and Mass Transfer* **1** 131
- [4] Craft T J, Launder B E and Suga K 1996 *International Journal of Heat and Fluid Flow* **17** (2) 108
- [5] Jones W P and Launder B E 1972 *International Journal of Heat and Mass Transfer* **15** 301
- [6] Baldwin B and Lomax H 1978 *Thin Layer Approximation and Algebraic Model for Separated Turbulent Flows* AIAA-78-257
- [7] Yang Z and Shih H 1993 *AIAA Journal* **31** (7) 1191
- [8] AGARD 1998 *CFD Validation for Propulsion System Components* AGARD-AR-355
- [9] Strazisar A J 1994 *Data Report and Data Diskette for NASA Transonic Compressor Rotor37* NASA Lewis Research Center
- [10] Shabbir A, Celestina M L, Adamczyk J J and Strazisar A J 1997 *The Effect of Hub Leakage Flow on Two High Speed Axial Flow Compressor Rotors* ASME Paper 97-GT-346
- [11] Hah C and Loellbach J 1997 *Development of Hub Corner Stall and its Influence on the Performance of Axial Compressor Blade Rows* ASME Paper 97-GT-42
- [12] Arnone A and Pacciani R January 1998 *Journal of Turbomachinery* **120** 147
- [13] Denton J D 1983 *ASME J. of Engineering for Power* **105** (3) 514
- [14] Patel V C, Rodi W and Scheuerer G 1985 *AIAA Journal* **23** (9) 1308
- [15] Wallscheid L and Eulitz F 1997 *Investigation of Rotor/Rotor Interaction* ISABE 97-7186
- [16] Wallscheid L, Eulitz F and Heinecke R 1998 *Investigation of Unsteady Flow Phenomena in a Counterrotating Ducted Propfan* ASME 98-GT-251
- [17] Wallscheid L 1999 *Phänomenologische Untersuchung der zeitabhängigen Strömung in einem gegenläufigen Propfan* DLR-Forschungsbericht 1999-24
- [18] Gerolymos G A and Vallet I 1997 *AIAA Journal* **35** 228

